Supplementary Information for

Asymmetric Toughening in the Lap Shear of Metamaterial Structural Adhesives

Chenghai Li[a], Qiang Guo[a], Robert Chambers[b], Shengqiang Cai[*a, b]

[a] Department of Mechanical and Aerospace Engineering, University of California, San Diego, La Jolla, CA 92093, USA.

[b] Materials Science and Engineering Program, University of California, San Diego, La Jolla, CA 92093, USA.

[*] Corresponding author. Email: s3cai@ucsd.edu (S.C.)

This PDF file includes:

Supplementary Table 1

Supplementary Text 1

Supplementary Figures S1 to S6

Other supplementary materials for this manuscript include the following:

Movies S1 to S8

Supplementary Table 1 Dimensions of various backing structures and the initial crack length in lap shear tests (unit: mm)

Group	b	s	N	t	θ (°)	L	H	w	C_0
1	1.9	4.8	12	2	26.6	82.6	10	8	15 in D1; 12 in D2
	2.4		10		45	77.2			14 in D1 and D2
	5.05		8		70.3	94.8			24 in D1; 17 in D2
2	7.2	4.8	8	0.5	45	101.2	8.5	10	17 in D1; 12 in D2
				0.75			8.75		
				1			9		
				1.5			9.5		
				2			10		
3	2.4	4.8	10	0.5	45	77.2	8.5	8	14 in D1 and D2
				0.75			8.75		
				1			9		
				1.5			9.5		
				2			10		
4	1.9	4.8	12	0.5	26.6	82.6	8.5	8	15 in D1; 12 in D2
	2.4		10		45	77.2			14 in D1 and D2
	5.05		8		70.3	94.8			24 in D1; 17 in D2

Supplementary Text 1

Effects of the terminated film thickness *t* on adhesion properties of MSAs with identical slender beams

We design the third group of MSAs with identical slender beams but varying *t* (see Fig. S4a and Table 1) and employ identical testing procedures across all samples. Our experimental results show that while the terminated film thickness *t* has minimal impact on the initial segment of force-displacement curves, it significantly affects the later portion (Fig. S4b). Notably, when the terminated film thickness is decreased from $t = 2\ mm$ to $t = 0.75\ mm$, the later segment of force-displacement curves shows moderate variations. However, further decreasing the film thickness to $t = 0.5\ mm$ leads to a dramatic increase of the maximum shear force, accompanied by a pronounced dispersion of the curves due to the random new crack initiations.

For a relatively thick terminated film ($t = 2\ mm$), the initial crack always propagates unidirectionally along the predefined path, exhibiting evident crack trapping behaviors. Conversely, for a relatively thin terminated film ($t = 0.5\ mm$), we always observe randomly initiated new cracks concurrent with the propagation of the initial crack. For an intermediate terminated film ($t = 0.75\ mm$), the initial crack always propagates unidirectionally along the predefined path, displaying clear crack trapping behaviors. While random new crack initiations may still occur, they are not discernible in our recorded videos.

Consequently, the normalized shear strength τ/τ_0 shows slight variations but is less conclusive with the decrease of t, ranging from $\sim 1.0 \pm 0.10$ at $t = 2\ mm$ to $\sim 0.60 \pm 0.14$ at $t = 0.75\ mm$ (Fig. S4c). With a further decrease to $t = 0.5\ mm$, τ/τ_0 becomes significantly larger and dispersed ($\sim 2.6 \pm 0.61$) due to randomly initiated new cracks. Meanwhile, the normalized adhesion energy Γ/W_{ad} demonstrates the same trend with the decrease of t, ranging from $\sim 1.7 \pm 0.16$ at $t = 2\ mm$ to $\sim 0.98 \pm 0.30$ at $t = 0.75\ mm$. Similarly, for a thin terminated film ($t = 0.5\ mm$), Γ/W_{ad} becomes obviously larger and dispersed ($\sim 10.4 \pm 2.1$) due to randomly initiated new cracks.

For a relatively large thickness ($t = 2\ mm$), the propagation of the initial crack follows the predefined path, and the shear strength and effective adhesion energy agree well with theoretical predictions based on the crack trapping mechanism (yellow circles in Fig. S4c and d). In contrast, for a relatively small thickness ($t = 0.5\ mm$), the propagation of the initial crack coexists with noticeable random new crack initiations. The shear strength is notably lower than theoretical predictions. Although the effective adhesion energy is close to theoretical predictions, these outcomes are incidental, arising from the failure of the crack trapping mechanism considering only the initial crack (yellow circles in Fig. S4c and d). In the intermediate thickness ranging from $t = 1.5\ mm$ to $t = 0.75\ mm$, we observed increasingly pronounced deviations between experiments and predictions for both τ/τ_0 and Γ/W_{ad} (Fig. S4c and d), which indicates a gradual transition between the two distinct crack propagation dynamics as mentioned above.

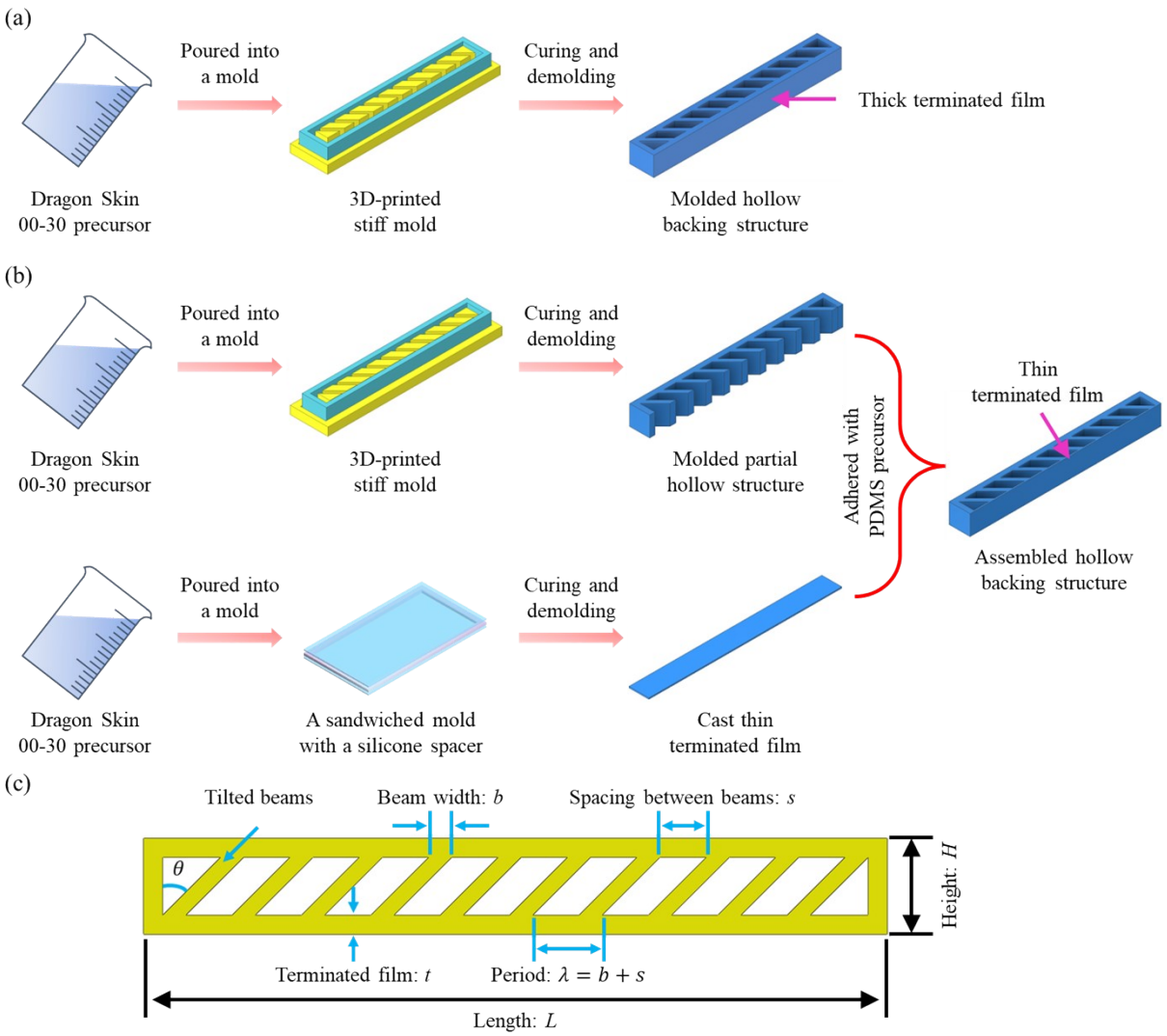

Fig. S1. Fabrication process and geometric parameters of the thick backing structure. (a) Dragon Skin 00-30 precursor was mixed, degassed, and then poured into a 3D-printed stiff mold to fabricate the hollow backing structure with a relatively thick terminated film ($t = 1, 1.5\ and\ 2\ mm$). (b) Dragon Skin 00-30 precursor was poured into a 3D-printed mold and a sandwiched mold to fabricate the partial hollow structure and a relatively thin terminated film ($t = 0.5\ and\ 0.75\ mm$), respectively. Subsequently, PDMS precursor was used to bond the thin terminated film with the partial hollow structure, which was left in a $60\ ^{\circ}C$ oven overnight for curing. Refer to **Experimental methods** for details. (c) Geometric parameters of the hollow structure. The width (w) of the hollow backing is perpendicular to the plane (not shown in the schematic).

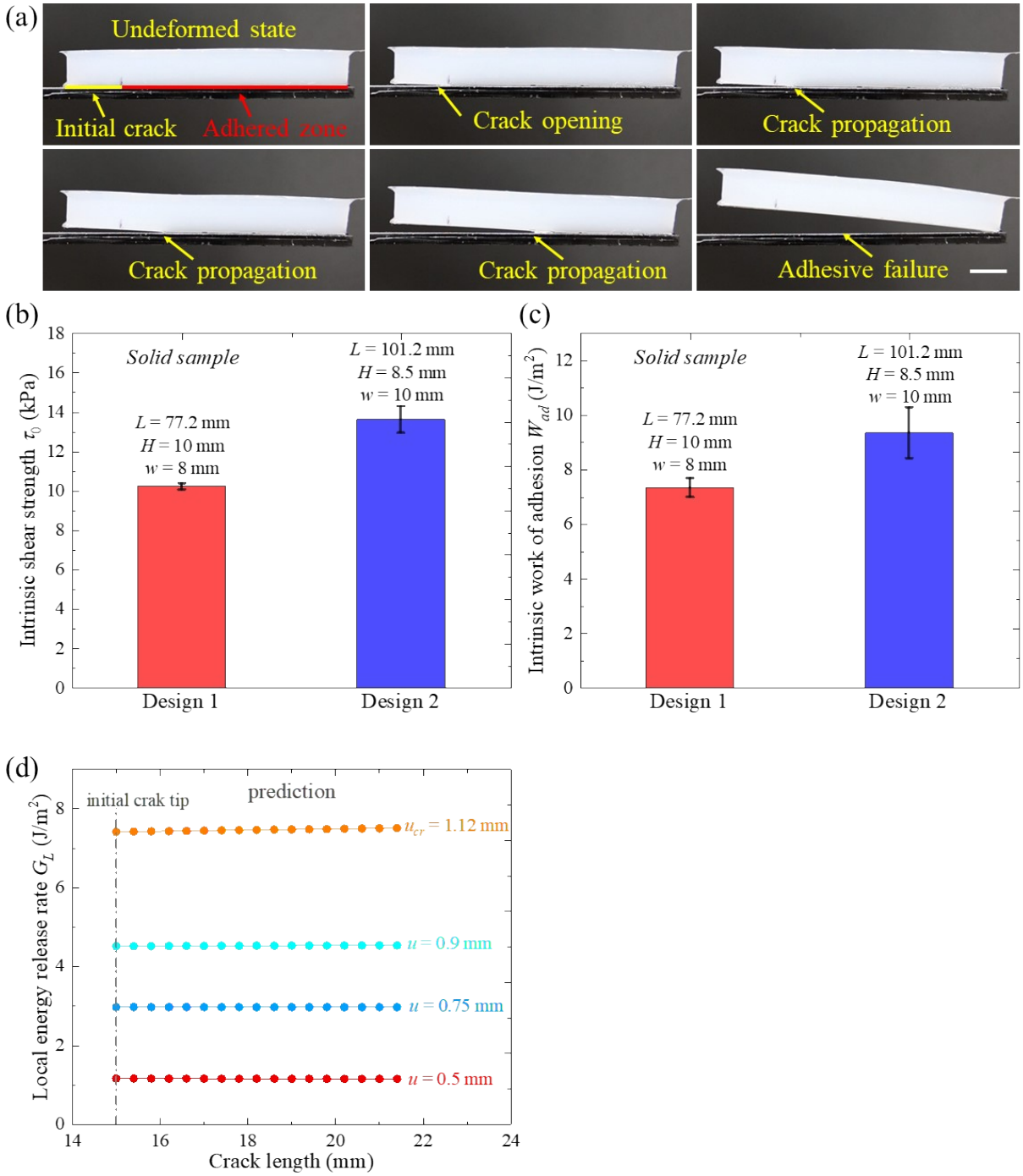

Fig. S2. Crack propagation dynamics and nearly size-independent intrinsic adhesion properties of the solid samples. (a) Representative images showing crack propagation dynamics. Scale bar, 1cm. The size effects of solid samples on the experimentally measured (b) intrinsic shear strength τ_0 and (c) intrinsic work of adhesion W_{ad}. (d) Numerically predicted G_L-crack length curves under various applied shear displacements.

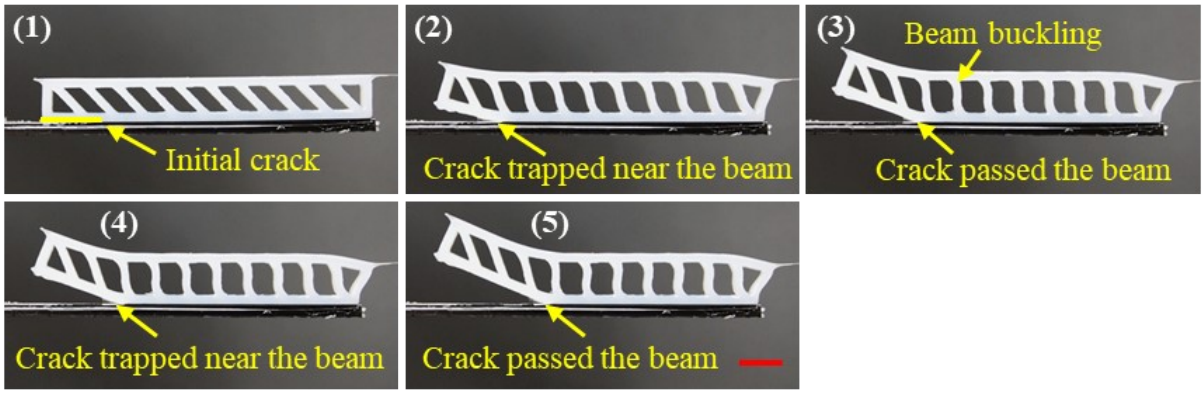

Fig. S3. Representative images showing the crack propagation dynamics of MSAs with slender beams and a thick terminated film tested in direction 1 ($b = 2.4\ mm$, $s = 4.8\ mm$, $t = 2\ mm$ and $\theta = 45°$). Scale bar, 1cm.

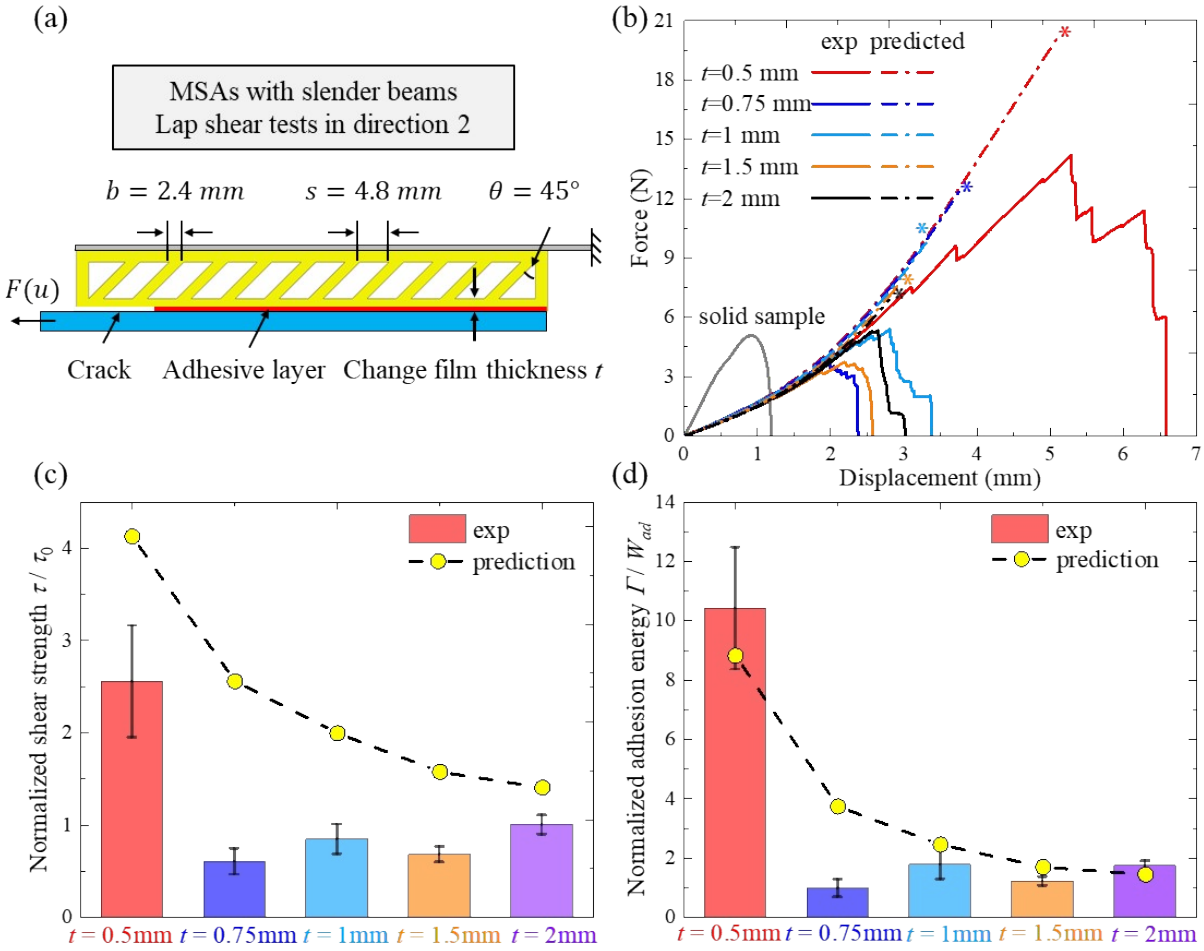

Figure S4. Effects of the terminated film thickness (*t*) on adhesion properties of MSAs with slender beams from both experimental measurements and theoretical predictions. (a) Schematic showing the lap shear test and geometric parameters of the MSAs with varied terminated film thickness *t*. (b) Effects of the terminated film thickness t on force-displacement curves of MSAs compared to the solid sample. Effects of the terminated film thickness t on the (c) normalized shear strength τ/τ_0 and (d) normalized adhesion energy Γ/W_{ad} of MSAs, respectively.

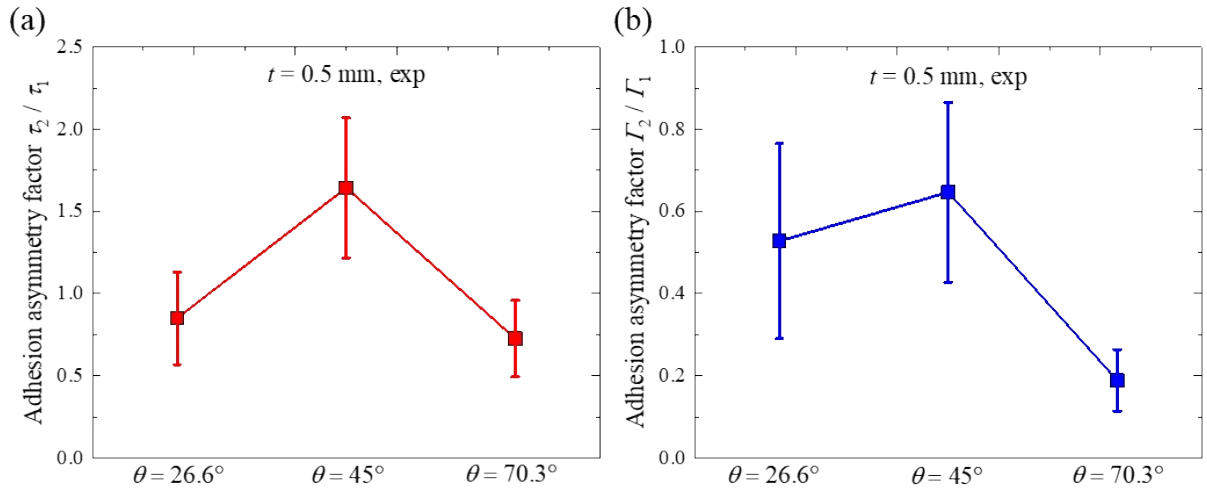

Fig. S5. Effects of the beam tilting angle θ on adhesion asymmetry factors (a) τ_2/τ_1 and (b) Γ_2/Γ_1 of MSAs with slender beams and a thin terminated film.

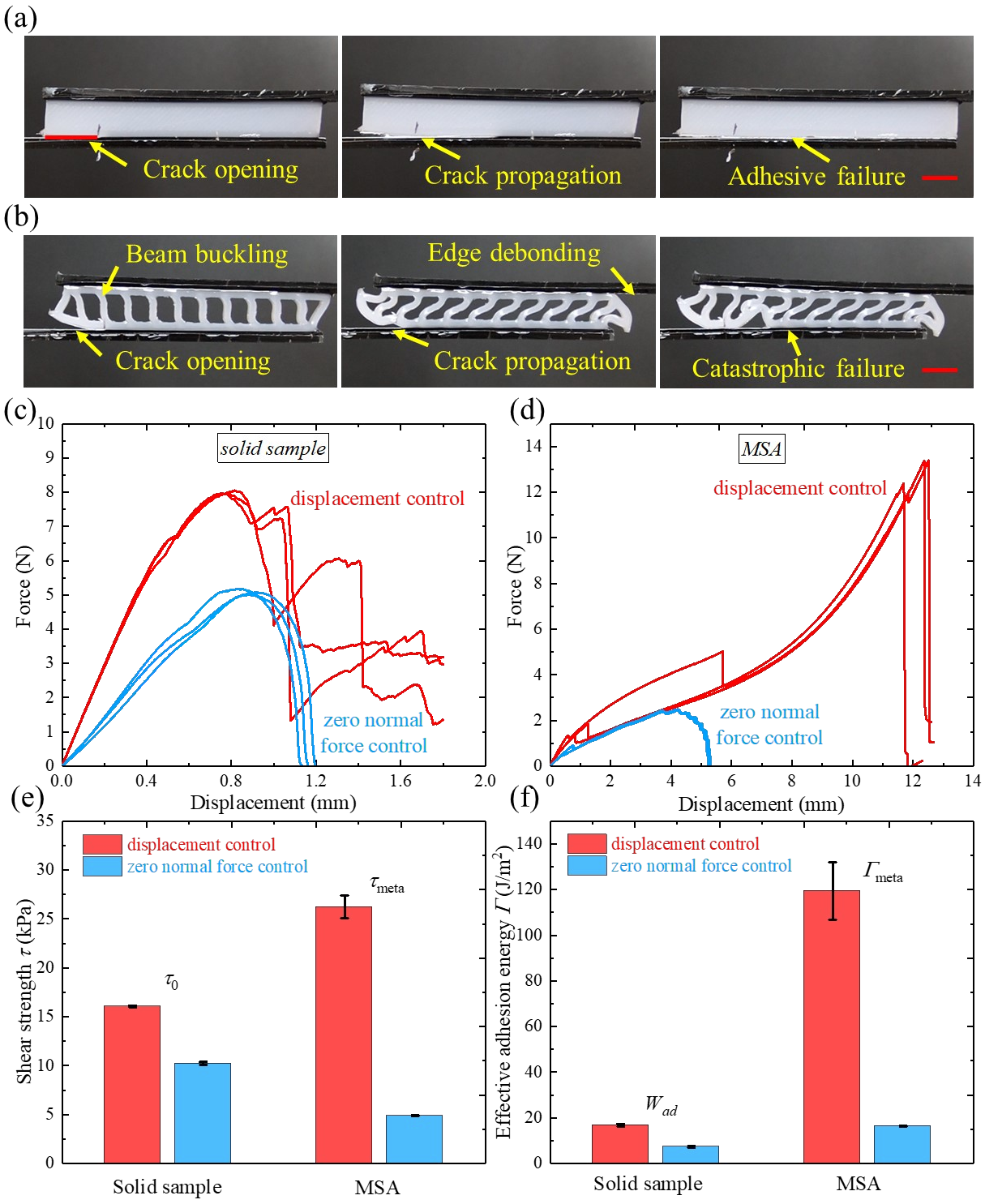

Fig. S6. Effects of the control modes normal to the lap shear direction on adhesion properties for both solid samples and MSAs. Representative images show crack propagation dynamics of (a) the solid sample and (b) the MSA under the displacement control mode. All scale bars are 1 cm. Effects of the control modes on force-displacement curves for (c) solid samples and (d) MSAs, respectively. Effects of the control modes

on the (e) shear strength τ and (f) effective adhesion energy Γ for both solid samples and MSAs, respectively.